THE EFFECT OF THE DIAMETER RATIO ON THE ABSOLUTE AND CONVECTIVE INSTABILITY OF FREE, COFLOWING JETS

A. Sevilla*, C. Martínez-Bazán* and J.M. Gordillo**
asevilla@ing.uc3m.es
***Área de Mecánica de Fluidos, Universidad Carlos III de Madrid.**
Avda. de la Universidad 30, 28911, Leganés (Madrid), Spain.
****Grupo de Mecánica de Fluidos, Escuela Superior de Ingenieros de Sevilla.**
Camino de los Descubrimientos s/n, 41092, Sevilla, Spain.

Abstract
The spatio-temporal stability analysis of free coaxial jets with finite diamater ratio is performed for the cases of negligible and non-negligible surface tension effects. A new mode of instability caused by the external shear layer is exhaustively studied, and transition diagrams between absolute and convective instability are built in a parameter space including density ratio, diameter ratio, velocity ratio and Weber number. This new mode is shown to considerably change the stability properties of the equivalent coaxial jet with infinite diameter ratio already studied in the literature. Preliminary experimental results show agreement with the stability calculations.

Introduction

Coflowing jets are of great relevance in many industrial applications such as atomization and aeration processes [1, 2, 3, 4]. The study of drop and bubble formation in this type of systems is crucial to control their size, velocity and production rate. It is generally accepted that the above mentioned parameters are mainly governed by the near field instabilities growing close to the nozzle. In recent experiments we have shown that, under certain conditions, there is a coupling effect between the outer mixing layer, which develops between the outer fluid and the quiescent environment, and the inner interface. This coupling effect displays the characteristics of globally unstable systems and, therefore, a region of local absolute instability is expected to exist in the near field [5, 6].

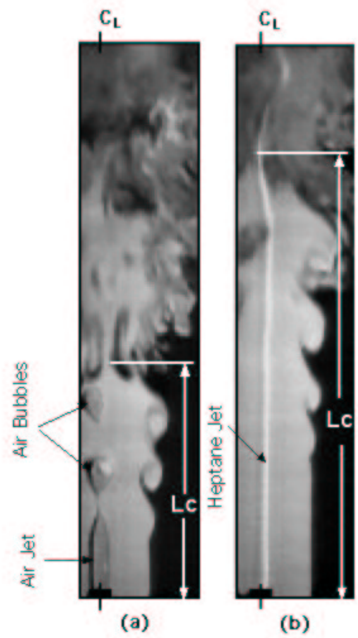

Figure 1: Experimental observations of two different coaxial jet configurations. (a) Air-water jet and, (b) heptane-water jet. C_L denotes the position of the jet axis.

The photographs shown in Fig. 1 are flow visualizations of well controlled coaxial-jet experiments where an inner jet is surrounded by an outer submerged water jet discharging upwards into a stagnant water tank. In both pictures, the outer water jet, seeded with fluoresceine dye, is visualized by the bright portion of the image when the flow is illuminated with a vertical 5 watts Argon-Ion laser sheet. However, the unseeded stagnant water contained in the reservoir does not glow and remains dark. The spatially developing outer mixing layer is observed to evolve due to the growth of the Kelvin–Helmholtz billows caused by the unstable velocity difference. In both images the outer–nozzle diameter is 3 mm, while the inner–jet diameter is 0.711 mm giving, therefore, a diameter ratio equal to 4.22. The mean water exit velocity is 2.67 m/s, which corresponds to a water jet Reynolds number $R_e \approx 8000$. As can be seen in Fig. 1, under certain conditions there is an important coupling effect between the inner interface and the outer jet mixing layer. In Fig. 1a, where the inner jet is air, $\rho_a/\rho_w \approx 1.2 \times 10^{-3}$, injected at the same mean velocity as the outer water jet, $U_a = U_w = 2.67$ m/s, we observe that the development of the Kelvin–Helmholtz waves is quite regular, and the length of the potential core, denoted by L_c, is considerably reduced compared to that of the single-phase jet. It may also be observed that the detachment of bubbles from the air ligament is in phase with the passage of mixing layer vortices. Notice that the two bubbles indicated in Fig. 1a are located nearly at the same downstream position as the corresponding large, coherent structures. Furthermore, the air-water system develops the oscillatory behavior of a self-excited system.

A completely different scenario is however depicted in Fig. 1b, where the inner fluid is heptane, $\rho_h/\rho_w \approx 0.8$, also injected at the same mean velocity as the water jet, $U_h = U_w = 2.67$ m/s. In this case the spatial evolution of the outer mixing layer is similar to that commonly observed in the single-phase jet, with a potential core longer than that observed in the air-water system of Fig. 1a. The inner jet reaches the end of the potential core before being perturbed and, consequently before being broken. Therefore, unlike the air-water system, which exhibits a coupling effect between the external mixing layer and the inner air jet, the outer shear layer and the inner interface are no longer synchronized in the heptane-water system.

These observations have led us to believe that, for some combinations of the control parameters (density ratio, velocity ratio, etc), a finite diameter ratio may deeply affect the evolution of the jets. If the self-excitation observed in the case of the air-water jet corresponds to an unstable global mode, local linear instability analysis must reveal local absolute instability of the coaxial jet flow. This analysis has been performed to compute transition diagrams between absolute and convective instability as function of the control parameters, i.e. density ratio (S), diameter ratio (a), velocity ratio (Λ) and Weber number (We). A hyperbolic-tangent like profile has been chosen for the calculations. This profile, already used in a number of publications [7], has the advantage of accurately describing the local flow within the whole potential core of high Reynolds number jets. For the sake of clarity, we have divided the study in two parts: first, the case with negligible surface tension effects was solved (We $\to \infty$), where the only cause of inviscid instability is the inflectional velocity profile resulting in a shear-layer type jet instability. Second, we performed the analysis for finite Weber numbers, where surface tension triggers Rayleigh-type instabilities. We will neglect gravitational forces by considering that they are much smaller than inertial ones. Furthermore, we will assume an inviscid evolution of the perturbed field, an aproximation known to be accurate for open, high Reynolds number flows under consideration.

Description and formulation of the problem

Here, cylindrical coordinates are denoted (z, r, ϕ), suffices 1 and 2 stand for magnitudes associated to the inner and outer streams respectively, and $p_{1,2}$ stands for the perturbed pressure field. The basic flow consists of an inner jet of radius R_1, velocity U_1 and density ρ_1, and a coflowing outer jet of radius R_2, velocity U_2 and density ρ_2 discharging into a stagnant fluid of the same density (Fig. 2). The unperturbed interface is a cylinder of radius R_1. As previously stated, we will assume the following basic parallel flow, which only depends on the radial coordinate r

$$\begin{aligned} \vec{U}(r) = \quad & \frac{U_2}{2}\left\{1 - \tanh\left[\frac{1}{4}\frac{R_2}{\tilde{\theta_2}}\left(\frac{r}{R_2} - \frac{R_2}{r}\right)\right]\right\} + \\ + \quad & \frac{U_1 - U_2}{2}\left\{1 - \tanh\left[\frac{1}{4}\frac{R_1}{\tilde{\theta_1}}\left(\frac{r}{R_1} - \frac{R_1}{r}\right)\right]\right\}\vec{e}_z\,. \end{aligned} \tag{1}$$

Following the above equation, the inner and outer shear layers are centered at $r = R_1$ and $r = R_2$, having momentum thicknesses $\tilde{\theta_1}$ and $\tilde{\theta_2}$ respectively.

The wavenumber, frequency and azimuthal number of instability modes are respectively denoted by k, Ω and m. We will use the dimensionless variables $\eta = r/R_1$ and $p_j = \bar{p}_j/\rho_1 U_1^2, j = 1, 2$, as well as the following set of global parameters: $\alpha = R_1 k$ (dimensionless wavenumber), $\beta = \Omega R_1/U_1$ (dimensionless frequency), $S = \rho_1/\rho_2$ (density ratio), $\Lambda = U_2/U_1$ (velocity ratio), $a = R_2/R_1$ (diameter ratio), $V(\eta) = U(r)/U_1$ (dimensionless

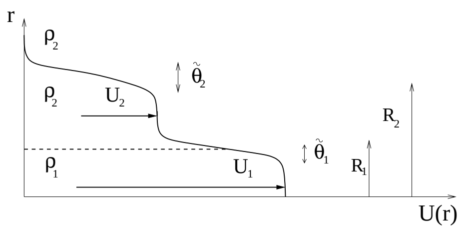

Figure 2: Scheme of the coaxial jet flow under study.

basic velocity profile), $\theta_1 = \tilde{\theta}_1/R_1$ (inner momentum thickness), $\theta_2 = \tilde{\theta}_2/R_1$ (outer momentum thickness), $\mathrm{We} = \rho_1 U_1^2 R_1/\sigma$ (Weber number).

With the above notation, it is easy to show that the linearized Euler equations can be simplified to the following eigenvalue problem for the perturbed pressure field:

$$\frac{d^2 p_{1,2}}{d\eta^2} + \left[\frac{1}{\eta} - \frac{2\,\alpha}{\alpha\, V(\eta) - \beta}\,\frac{dV}{d\eta}\right]\,\frac{dp_{1,2}}{d\eta} - \left(\alpha^2 + \frac{m^2}{\eta^2}\right)\, p_{1,2} = 0\,, \tag{2}$$

where the basic flow takes the form

$$\begin{aligned} V\,(\eta) \;&= \tfrac{\Lambda}{2}\left\{1 - \tanh\left[\tfrac{a}{4\,\theta_2}\left(\tfrac{\eta}{a} - \tfrac{a}{\eta}\right)\right]\right\} + \\ &+ \tfrac{1-\Lambda}{2}\left\{1 - \tanh\left[\tfrac{1}{4\,\theta_1}\left(\eta - \tfrac{1}{\eta}\right)\right]\right\}\,. \end{aligned} \tag{3}$$

The boundary conditions are

$$\left\{\begin{array}{ll} \eta = 0 & p_1 \neq \infty \\ \eta \to \infty & p_2 \to 0\,, \end{array}\right. \tag{4}$$

and

$$\eta = 1:\;\left\{\begin{array}{l} p_1 = p_2 + \mathrm{We}^{-1}(\alpha^2 + m^2 - 1)p_1'/(\alpha V_s - \beta)^2 \\ p_1' = S p_2'\,. \end{array}\right. \tag{5}$$

where V_s is the value of axial velocity at the interface, and a prime denotes differentiation with respect to η.

The numerical procedure used to solve the eigenvalue problem (2)–(5) is based on a shooting method combined with a Newton-Raphson iterative scheme for fast convergence. We start integrating Eq. (2) from both a point near the axis and a point far from the central line where the mixing layers have already relaxed to an almost uniform profile. The values of pressure perturbation at these points are estimated using the asymptotic expression of Eq. (2) for uniform profiles, and we impose the linear dependence of the inner and the outer solutions at some point between the interface and the mixing layer. This condition provides an equation of the form $D\,(\alpha, \beta;\, m, \theta_1, \theta_2, a, S, \Lambda) = 0$, which constitutes the dispersion relation to be satisfied in order to obtain non-trivial solutions. To locate points of zero group velocity, $d\beta/d\alpha\,\left(\alpha^0\right) = 0$, the two simultaneous equations to satisfy are

$$\left\{\begin{array}{l} D\left(\alpha^0, \beta^0; m, \theta_1, \theta_2, a, S, \Lambda\right) = 0 \\ \dfrac{\partial D}{\partial \alpha}\left(\alpha^0, \beta^0; m, \theta_1, \theta_2, a, S, \Lambda\right) = 0\,. \end{array}\right. \tag{6}$$

The first expression in Eq. (6) is the dispersion relation, and the second equation represents one of the forms to express the nullity of the complex group velocity, i.e., the existence of a saddle-point in the complex wavenumber plane (α–plane). The values of wavenumber and frequency at the saddlepoint, $\left(\alpha^0, \beta^0\right)$, are generally called *absolute wavenumber* and *absolute frequency* respectively.

Results for the limit We $\to \infty$

In the case of negligible surface tension effects, two relevant instability modes have been identified, namely, PI associated to the inner shear layer, and PII associated to the outer one. The PI mode, commonly known as the *light jet* or *hot jet* mode, has been extensively investigated in the past in the $a \to \infty$ limit [8, 9, 10, 11, 12, 13]. Earlier

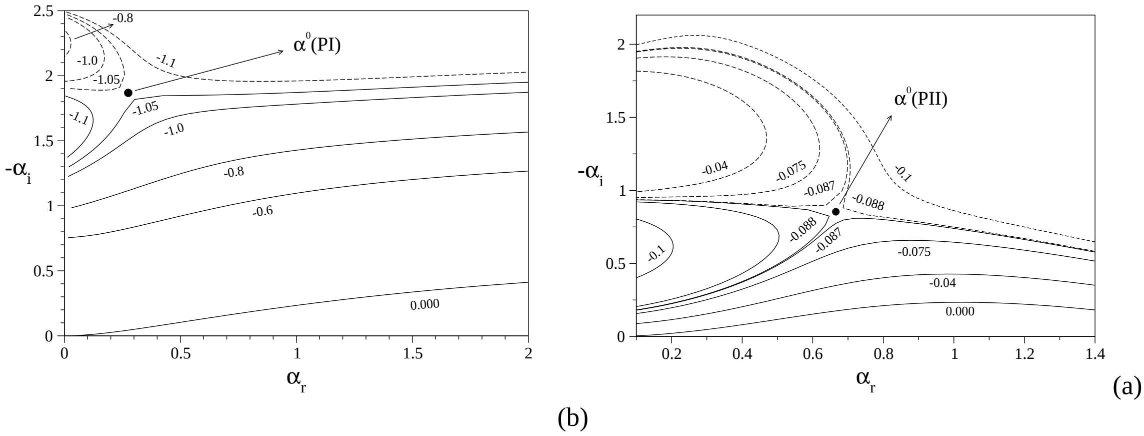

Figure 3: (a) Level curves $\beta_i = $ const. in the α–plane showing pinch-point PI, associated with the inner mixing layer. $m = 0$, $\theta_1 = 0.06$, $\theta_2 = 0.24$, $S = 1$, $\Lambda = 0.5$, $a = 2$. (b) Same as Fig. 3a showing pinch-point PII, associated with the outer mixing layer. $m = 0$, $\theta_1 = 0.06$, $\theta_2 = 0.24$, $S = 1$, $\Lambda = 0.5$, $a = 2$.

results obtained for the light–jet configuration [8, 10, 12], which in this study corresponds to the limit $a \to \infty$, show a transition to absolute instability in the $m = 0$ mode when the inner stream is sufficiently lighter than the outer one, and the outer coflow is slow enough. Figures 3a and 3b show the pinch–points, hereafter named PI and PII, associated respectively to modes PI and PII for the following values of the dimensionless control parameters: $m = 0$, $\theta_1 = 0.06$, $\theta_2 = 0.24$, $S = 1$, $\Lambda = 0.5$, $a = 2$. The numbers shown on the spatial branches correspond to the values of the imaginary part of β. It is clearly observed that the branch-exchange process fulfills the Briggs–Bers criterion. Pinch–points PI and PII can be naturally assigned to the inner and the outer shear layers respectively. Since PI is the mode associated with the inner shear layer, it is the only mode present for large values of a. This mode has already been described in the literature, whereas mode PII, was first analyzed by Sevilla et al. [6]. The

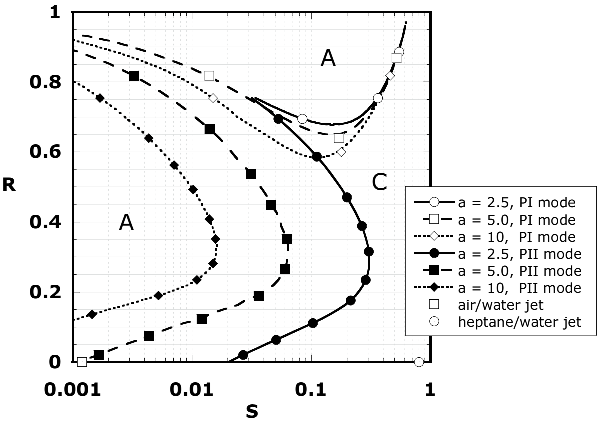

Figure 4: We $\to \infty$ transition diagram in the R-S plane for several values of a, where $R = (1-\Lambda)/(1+\Lambda)$. Here $\boxdot$ represents the air-water jet of Fig. 1a, and $\odot$ represents the heptane-water jet of Fig. 1b.

transition diagram of Fig. 4 shows that, for a given value of a, there are two different curves which correspond to modes PI and PII respectively. This pair of curves divides the R-S parameter plane into several C/A unstable regions. Notice that in this diagram the C/A transition can be triggered by either modes PI or PII. The curves with solid symbols indicate the C/A transition line caused by mode PII while the curves with open symbols display the C/A transition promoted by mode PI. Let us classify the regions presented in Fig. 4. For values of $S > 0.7$ the flow is always convectively unstable, independently of the values of R and a. The C/A transition controlled by mode PI is only possible for sufficiently large values of R, $R \geq 0.57$. Furthermore, our study reveals that, in practical applications where a is finite ($a \leq 10$), the system may exhibit an absolute instability caused by mode PII. Observe that there exists an optimum value of the coflow parameter, $R \sim 0.3$, nearly independent of a, for which the system becomes absolutely unstable due to the effect of mode PII.

The point corresponding to the air-water jet is represented by ⊡ while the point associated with the heptane-water jet is indicated by ⊙. It may be observed that the present investigation qualitatively corroborates the C/A nature of both systems. The analysis presented here shows a convectively unstable flow for the heptane-water jet (S=0.8), while it predicts an absolute instability for the air-water jet (S=1.2 × 10^{-3}). These results are apparent in Fig. 4 where it is observed that the air-water jet, indicated by ⊡, is within the absolutely unstable region of the $a = 4.22$ transition curve, while the heptane-water jet, ⊙, falls inside the convectively unstable zone. Therefore, the effect of the diameter ratio is more noticeable in the lighter, air-water configuration, triggering the absolute instability. However, at this point we cannot extract any quantitative conclusion for the finite surface tension situations shown in Fig. 1. This point will be addressed in the following section.

Results for finite Weber numbers

For finite Weber numbers a new instability mode caused by surface tension effects, hereafter named PC, is present in the flow. Figure 5a shows the We-a transition diagram for an air-water coflowing jet. In this figure, it can be observed that, as the Weber number tends to infinity, the results of the previous section are recovered: mode PII is convectively unstable for $a > 5$ and absolutely unstable otherwise. The transition from convective to absolute instability is dominated by this inertial mode for low values of a.

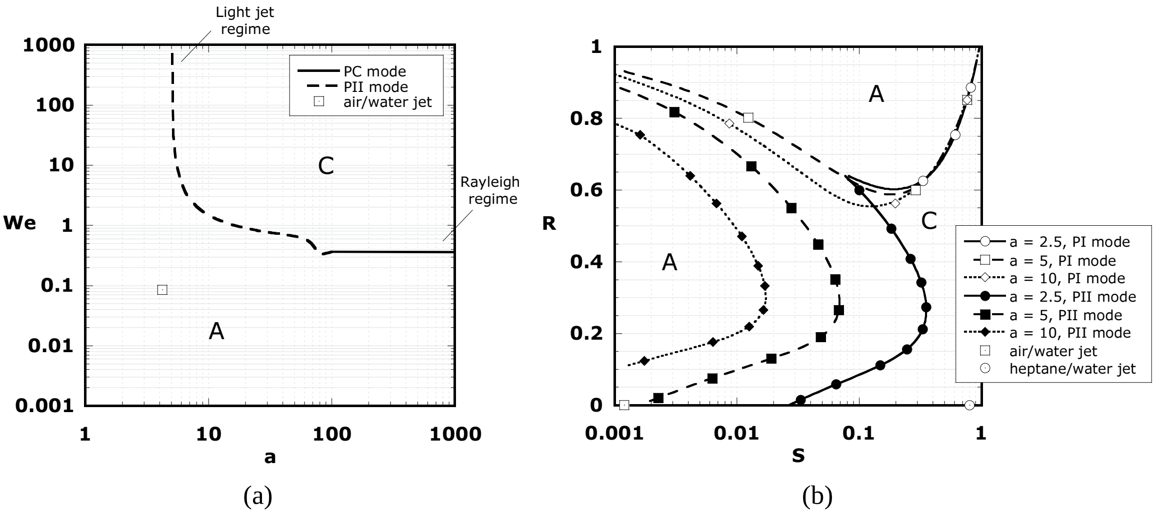

Figure 5: (a) Transition diagram in the We-a plane for the air-water jet ($S = 0.0012$) with no shear at the interface ($\Lambda = 1$). (b) We $= 10$, transition diagram in the R-S plane for several values of a. Here ⊡ represents the air-water jet of Fig. 1a, and ⊙ represents the heptane-water jet of Fig. 1b.

Moreover, as a is increased, the transition of the PII mode occurs at lower values of We, until a value of a where PII and PC transition curves cross is reached, $a_c \approx 80$. For values of a larger than a_c, the capillary mode PC becomes the dominant one, indicating that the transition is driven by surface tension effects. In the limit $a \to \infty$, the transitional Weber number of the air-water capillar jet without shear is recovered, We ≈ 0.35.

Figure 5b shows the R-S transition diagram for We $= 10$. The reason why there is no transition curve associated to PC is that, for this value of the Weber number is high enough for the mode PC to be always convectively unstable independently of the values of the diameter and velocity ratios. Nonetheless, there are some quantitative differences between Figs. 4 and 5b: the minimum density ratio for the system to be convectively unstable for any value of R is larger in the case We $= 10$, reaching a value of almost unity. Furthermore, it can be observed that all the transition curves move to the right of the diagram, i.e. to larger values of density ratio. These observations indicate that surface tension promotes the self-excited behaviour of PI and PII modes. For lower values of We, a completely different transitional scenario, currently under study, appears in the coaxial-jet flow.

Conclusions

We have discussed the influence of the outer shear layer on the instability characteristics of finite diameter ratio coaxial jets by computing the spatio-temporal response of the flow. Finite diameter ratios profoundly affect the non-stationary development of the flow, leading to predictions qualitatively and quantitatively different from infinite-coflow studies. This may be relevant for a better control of coaxial-jet near-field dynamics, and thus for a better control of atomization and mixing processes.

In the limit We $\rightarrow \infty$, a new region of absolute instability, caused by the effect of the external mixing layer, has been described in the present work. Such a region is always present in practical situations, since coflowing jets necessarily have a *finite* diameter ratio, commonly smaller than 10. The main features extracted from the study of the limit We $\rightarrow \infty$ are shown in figure 4: the Kelvin–Helmholtz-like mode PII, caused by the outer shear layer, becomes absolutely unstable for low enough density ratios and intermediate velocity ratios. These facts lead to the appearance of new absolutely unstable regions in the R-S parameter plane, which may be of relevance for control of coaxial-jet break-up and mixing.

In situations where surface tension effects cannot be neglected (i.e. low enough Weber numbers), the outer shear layer has a pronounced influence on the system. In the case of an air-water system without shear at the interface, we have seen that the nature of the instability is controlled by the inertial effects of the outer layer for values of the diameter ratio smaller than ~ 80, being surface tension effects the dominant influence otherwise. A detailed computation of the R-S transition diagram for We $= 10$ shows the same qualitative behaviour than the equivalent We $\rightarrow \infty$ case, indicating that values of We $\gtrsim 10$ surface tension effects become almost negligible.

It has been shown that experiments qualitatively corroborate the results extracted from the stability computations. In order to evaluate their quantitative accuracy, a detailed experimental study, including measurements of frequencies, wavelenths and growth rates is needed, and will be the subject of future work.

References

[1] S.P. Lin and R.D. Reitz. Drop and spray formation from a liquid jet. *Annu. Rev. Fluid Mech.*, 30:85–105, 1998.

[2] J.C. Lasheras and E.J. Hopfinger. Liquid jet instability and atomization in a coaxial gas stream. *Annu. Rev. Fluid Mech.*, 32:275–308, 2000.

[3] J.M. Gordillo, M. Pérez-Saborid, and A.M. Ganán-Calvo. Linear stability of co-flowing liquid–gas jets. *J. Fluid Mech.*, 448:23–51, 2001.

[4] A. Lozano, F. Barreras, G. Hauke, and C. Dopazo. Longitudinal instabilities in an air-blasted liquid sheet. *J. Fluid Mech.*, 437:143–173, 2001.

[5] P. Huerre. Open shear flow instabilities. In G. Batchelor, K. Moffatt, and G. Worster, editors, *Perspectives in fluid dynamics*, pages 159–229. Cambridge, 2000.

[6] A. Sevilla, J.M. Gordillo, and C. Martínez-Bazán. The effect of the diameter ratio on the absolute and convective instability of free, coflowing jets. *Accepted in Phys. Fluids*, 2002.

[7] D.G. Crighton and M. Gaster. Stability of slowly divergent jet flow. *J. Fluid Mech.*, 77:397–413, 1976.

[8] P.A. Monkewitz and K.D. Sohn. Absolute instability in hot jets. *AIAA J.*, 28:911–916, 1988.

[9] P.A. Monkewitz, D.W. Bechert, B. Barsikow, and B. Lehmann. Self-excited oscillations and mixing in a heated round jet. *J. Fluid Mech.*, 213:611–639, 1990.

[10] M.-H. Yu and P.A. Monkewitz. The effect of nonuniform density on the absolute instability of two-dimensional inertial wakes and jets. *Phys. Fluids A*, 2:611–639, 1990.

[11] M.-H. Yu and P.A. Monkewitz. Oscillations in the near field of a heated two-dimensional jet. *J. Fluid Mech.*, 25:323–347, 1993.

[12] S. Jendoubi and P.J. Strykowski. Absolute and convective instability of axisymmetric jets with external flow. *Phys. Fluids*, 6:3000–3009, 1994.

[13] D.W. Lim and L.G. Redekopp. Absolute instability conditions for variable density, swirling jets flows. *Eur. J. Mech. B/Fluids*, 17:165–185, 1998.